CORROSION SCIENCE AND TECHNOLOGY, Vol.6, No.1(2007), pp.1~6

Evaluation of STS 430 and STS 444 for SOFC Interconnect Applications

S. H. Kim, † J. Y. Huh, J. H. Jun[1], D. H. Kim[1], and J. H. Jun[1]

Department of Materials Science and Engineering, Korea University, Seoul 136-713, Korea
[1]New Materials & Components Research Center,
Research Institute of Industrial Science and Technology, Pohang 790-330, Korea

Ferritic stainless steels for the SOFC interconnect applications are required to possess not only a good oxidation resistance, but also a high electrical conductivity of the oxide scale that forms during exposure at the SOFC operating environment. In order to understand the effects of alloying elements on the oxidation behavior of ferritic stainless steels and on the electrical properties of oxide scales, two kinds of commercial ferritic stainless steels, STS 430 and STS 444, were investigated by performing isothermal oxidations at 800 ℃ in a wet air containing 3% H_2O. The results showed that STS 444 was superior to STS 430 in both of the oxidation resistance and the area specific resistance. Although STS 444 contained a less amount of Mn for the $(Mn,Cr)_3O_4$ spinel formation than STS 430, the minor alloying elements of Al and Mo in STS 444, which were accumulated in the base metal region adjacent the scale, were suggested to reduce the scale growth rate and to enhance the scale adherence to the base metal.

Keywords *: ferritic stainless steels, SOFC interconnect, oxidation, area specific resistance*

1. Introduction

Solid oxide fuel cells (SOFCs) are electrochemical devices that produce electricity by combining a fuel gas and an oxidizing gas (typically air) across a solid oxide electrolyte membrane with high conversion efficiency. Because of their high power densities, low emissions of pollutants, and the possibility to use a variety of fuels (such as hydrogen, methane, or natural gases), SOFCs have long been considered for applications as auxiliary power unit for vehicles as well as primary power source for distributed residences.[1),2)]

With the development of planar-type anode-supported SOFCs that can operate at temperatures below 800 ℃, ferritic stainless steels are now considered to be among the most preferred candidate materials for the interconnects in SOFC stacks, due to their electrically conducting oxide scale, appropriate thermal expansion behavior, low material cost, and excellent formability.[2),3)] However, the continuous growth of oxide scales in the SOFC operating environment, which increases the electrical resistance and thereby degrades the stack performance, is one of the major hurdles remaining to be overcome for the use of ferrite stainless steels as interconnect materials.[2)] Therefore, to ensure the reliability of the SOFC interconnects, it is desirable to develop a ferrite stainless steel whose scale exhibits a lowered growth kinetics and enhanced electrical conductivity in the SOFC operating environment.

Although the oxidation behavior of ferritic stainless steels has been extensively studied for various heat treatment conditions,[1)-7)] there still remain unclear points about the growth kinetics and electrical properties of the scales formed in the SOFC operating environment. To improve our understanding of the effects of alloying elements on the oxidation behavior of ferritic stainless steels and on the electrical properties of oxide scales, two kinds of commercial ferritic stainless steels, STS 430 and STS 444, were investigated by performing isothermal oxidations at 800 ℃ in a wet air (3% H_2O). The oxidation kinetics and the corresponding changes in the area specific resistance (ASR) are discussed in terms of the microstructure of the oxide scales and the alloying elements.

2. Experimental methods

The two kinds of ferritic stainless steels (namely, STS 430 and STS 444) employed in the present study were provided by POSCO in the form of 0.6 mm (STS 430)

† Corresponding author: jyhuh@korea.ac.kr

Table 1. Chemical compositions (wt.%) of the ferrite stainless steels provided by POSCO

STS	Fe	Cr	Mn	Ni	Mo	Ti	Si	C	Cu	Al	P	S
430	bal.	16.23	0.39	0.1	0.21	0	0.28	0.047	0.02	0.003	0.02	0.004
444	bal.	18.59	0.24	0.21	1.96	0	0.26	0.006	0.04	0.048	0.02	0.001

and 0.8 mm (STS444) thick foils. The detailed chemical compositions of these alloys are listed in Table 1. It is noted that the major difference between the two alloys, other than the Cr composition, occurs in the compositions of Mn, Mo and Al. The as-received foils were cut into 20×20 mm^2 square samples, polished on both sides using 1200 grit SiC sandpaper, and then ultrasonically cleaned in acetone. The oxidation experiments of the cleaned specimens were carried out at 800 ℃ for times up to 800 h in a tube furnace with a steady flow of wet air, simulating the cathode environment of SOFC operation. The wet air containing about 3% H_2O was prepared by passing ambient air through a porous stone bubbler in water held at 25 ℃.

The oxidation rate was determined by measuring the weight gains of the oxidized samples with an accuracy of 1×10^{-4} g. Each of the reported values of the weight gain per surface area was obtained by averaging the values from four samples. The surface microstructure of the scales was examined by a field-emission scanning electron microscope (FESEM) equipped with an energy dispersive X-ray (EDX) analyzer. The phase analyses of the oxide scales were performed by X-ray diffraction (XRD) using Cu-K_α radiation at an acceleration voltage of 50 kV. The depth profiling of the elemental distribution in the oxide scales was also carried out using a glow discharge spectrometry (GDS).

The electrical properties of the scales formed after oxidation were determined by measuring the area specific resistance (ASR) using a two-point, four-wire probe technique. For the ASR measurement, Pt contact layers on both surfaces of the oxidized samples were first formed by coating Pt paste and by baking at 800 ℃ for 1 h. Then, Pt meshes, each welded with two Pt measurement wires, were attached on both sides of the samples by using Pt paste and followed by another baking step at 800 ℃ for 1 h. The oxidized sample with Pt meshes attached on both sides was loaded in a muffle furnace and the ASR measurements were conducted in ambient air at 800 ℃ by measuring the voltage drop (V) across the sample thickness with increasing the current density (i) up to 200 mA/cm^2. To improve the contact on the scale, a dead load of 4.9×10^4 Pa was applied to the Pt meshes throughout the ASR test. Since the stainless steels have much lower resistivities than their oxides, the voltage drop is essentially attributed to the scales formed on both sides of the sample. Thus, the ASR values of the scales was calculated according to Ohm's law, $ASR=V/2i$, where the factor 2 accounts for the fact that the scales formed on both surfaces of the samples.

3. Results and discussion

During the exposure to the wet air at 800 ℃, the alloy specimens experience an increase in mass as a result of the scale formation by the selective reaction of metallic elements in the alloys with oxygen in air. Fig. 1 shows the weight gains (δw) of STS 430 and STS 444 as functions of the square root of oxidation time ($t^{1/2}$) at 800 ℃, indicating that both of the ferritic stainless steels exhibited parabolic scale growth by following $\delta w=(k_g t)^{1/2}$. The parabolic rate constant of the scale growth for STS 444, $k_g=2.07\times10^{-14}$ $g^2cm^{-4}s^{-1}$, was lower than that for STS 430, $k_g=3.77\times10^{-14}$ $g^2cm^{-4}s^{-1}$, demonstrating that STS 444 is more oxidation-resistant than STS 430 in the cathode environment of SOFC operation. As compared to the previously reported values of $k_g=35\times10^{-14}$ $g^2cm^{-4}s^{-1}$ for STS 430 in air oxidation at 800 ℃,[5] the present results of k_g are surprisingly small but the reason for this discrepancy is unclear at this point. The values of k_g for STS 430 and STS 444 are even lower than Crofer22 APU ($k_g=7.96\times10^{-14}$ $g^2cm^{-4}s^{-1}$) specially developed for SOFC

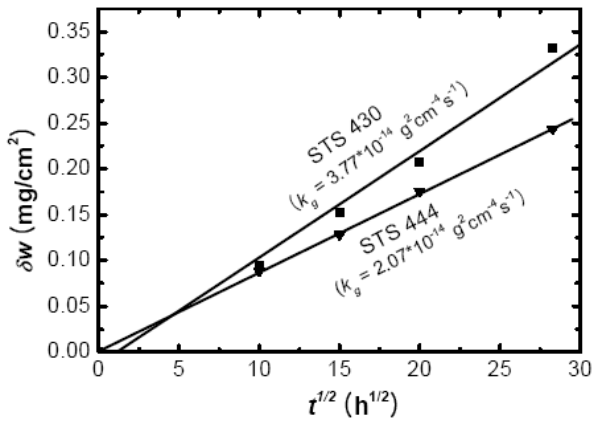

Fig. 1. Plots of weight gain versus oxidation time in a wet air (3% H_2O) at 800℃ for STS 430 and STS 444.

interconnect applications and they are comparable to E-brite (k_g=3.53×10^{-14} g^{2}cm^{-4}s^{-1}) that has a high Cr content of 27 wt.%.[6] It is noted that, in contrast to STS 444, scale delamination was observed in some oxidized samples of STS 430. This indicates that the scale grown on STS 444 has a better adherence to the ferrite substrate than that grown on STS 430.

Fig. 2(a) and (b) show the evolution of the XRD patterns of STS 430 and STS 444, respectively, with oxidation time at 800 ℃. With increasing oxidation time, the intensity of the ferrite substrate peaks decreased whereas that of the scale peaks increased, indicating that the scale grew thicker on the alloy surface. Pattern indexing revealed that the surface scales formed on the both alloys consisted of Cr_2O_3 corundum and $(Mn,Cr)_3O_4$ spinel based on the $MnCr_2O_4$ structure. As the oxidation time was increased from 225 h to 800 h, the peaks of the corundum and spinel phases became stronger in both alloys. However, from the change in the peak intensity ratios between the $(Mn,Cr)_3O_4$ spinel and Cr_2O_3, it is noted that, after 800 h, the $(Mn,Cr)_3O_4$ spinel was better developed in the scale grown on STS 430 than in the scale grown on STS 444. This is most likely due to the fact that, as listed in Table 1, STS 430 has a higher Mn content than STS 444.

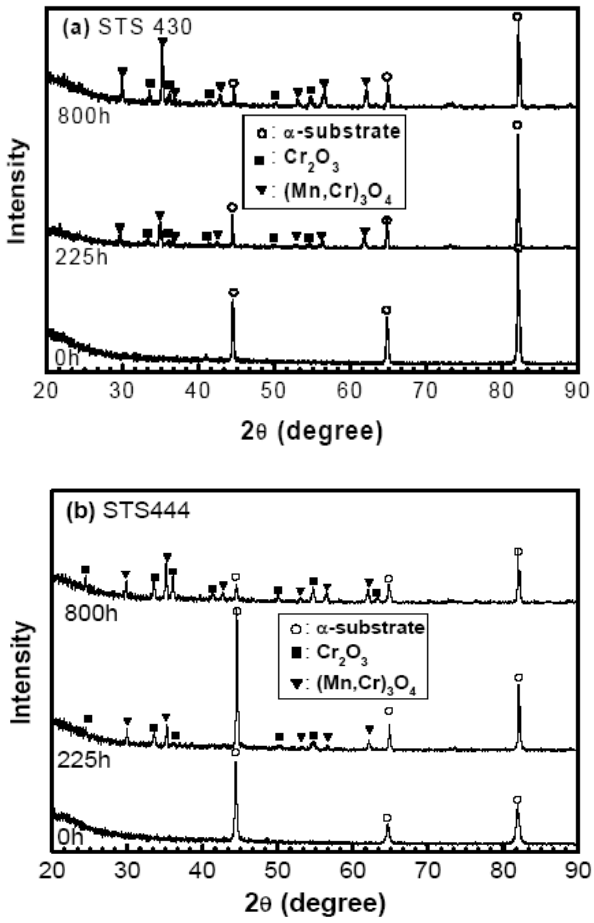

Fig. 2. XRD patterns of the scales grown on (a) STS 430 and (b) STS 444 after oxidation at 800℃ for 225 and 800 h. As a reference, the XRD pattern obtained prior to the oxidation is also shown.

In addition to the XRD analysis, the surface scales of oxidized specimens were further examined under SEM. Fig. 3 and 4 show the surface microstructures of the scales formed on STS 430 and STS 444, respectively. Overall, the surface of the scale grown on STS 444 was more uniform and smoother than that on STS 430. In the early stages of oxidation, as shown in Fig. 3(a) and 4(a) for 225 h of oxidation, the scales exhibited two different oxide particle morphologies: coarse angular particles distributed discontinuously on top of a continuous sublayer comprised of fine particles. The EDX analyses revealed that the coarse angular particles primarily contained Cr, Mn, and O, indicating that they are $(Mn,Cr)_3O_4$ spinel. The atomic ratio of Mn to Cr in the spinel particles was consistently greater for the case of STS 430, being close to 0.5 for the case of STS 444 shown in fig. 4(a) and about 0.8 for the case of STS 430 shown in Fig. 3(a). The fine particles forming a continuous sublayer mainly contained

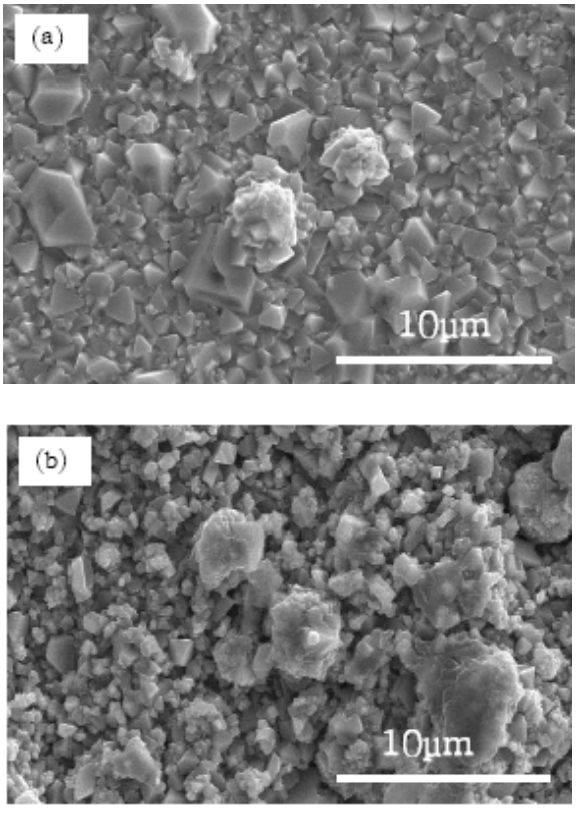

Fig. 3. SEM micrographs showing the surface morphology of the oxide scales grown on STS 430 after oxidation at 800℃ for (a) 225 and (b) 800 h.

Cr and O, with small amounts (several atomic percents) of Mn and minor amounts of Fe, and were likely $(Cr,Mn)_2O_3$ corundum.

The scales exhibited a drastic change in surface microstructure as the oxidation time was increased to 800 h. In the early stages of oxidation, STS 430 showed coarse angular spinel particles embedded partially in a continuous corundum sublayer, as shown in Fig. 3(a) for 225 h of

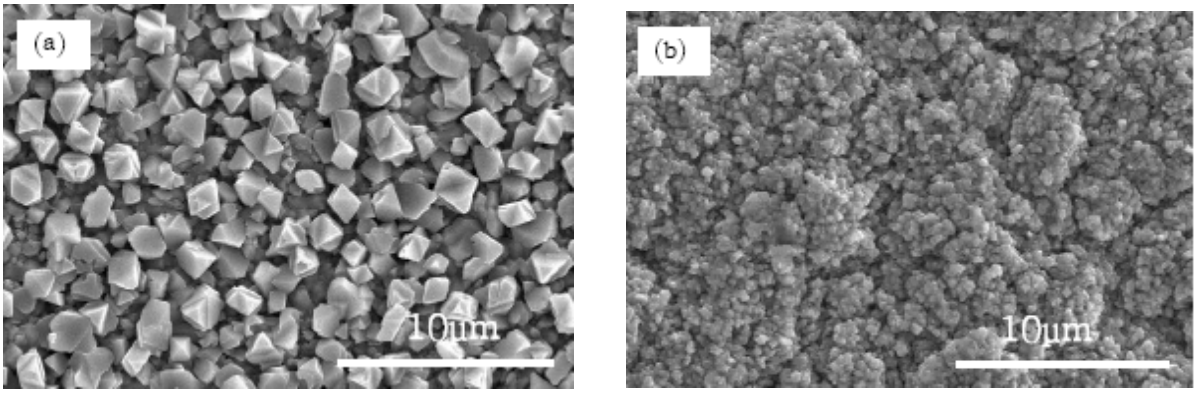

Fig. 4. SEM micrographs showing the surface morphology of the oxide scales grown on STS 444 after oxidation at 800℃ for (a) 225 and (b) 800 h.

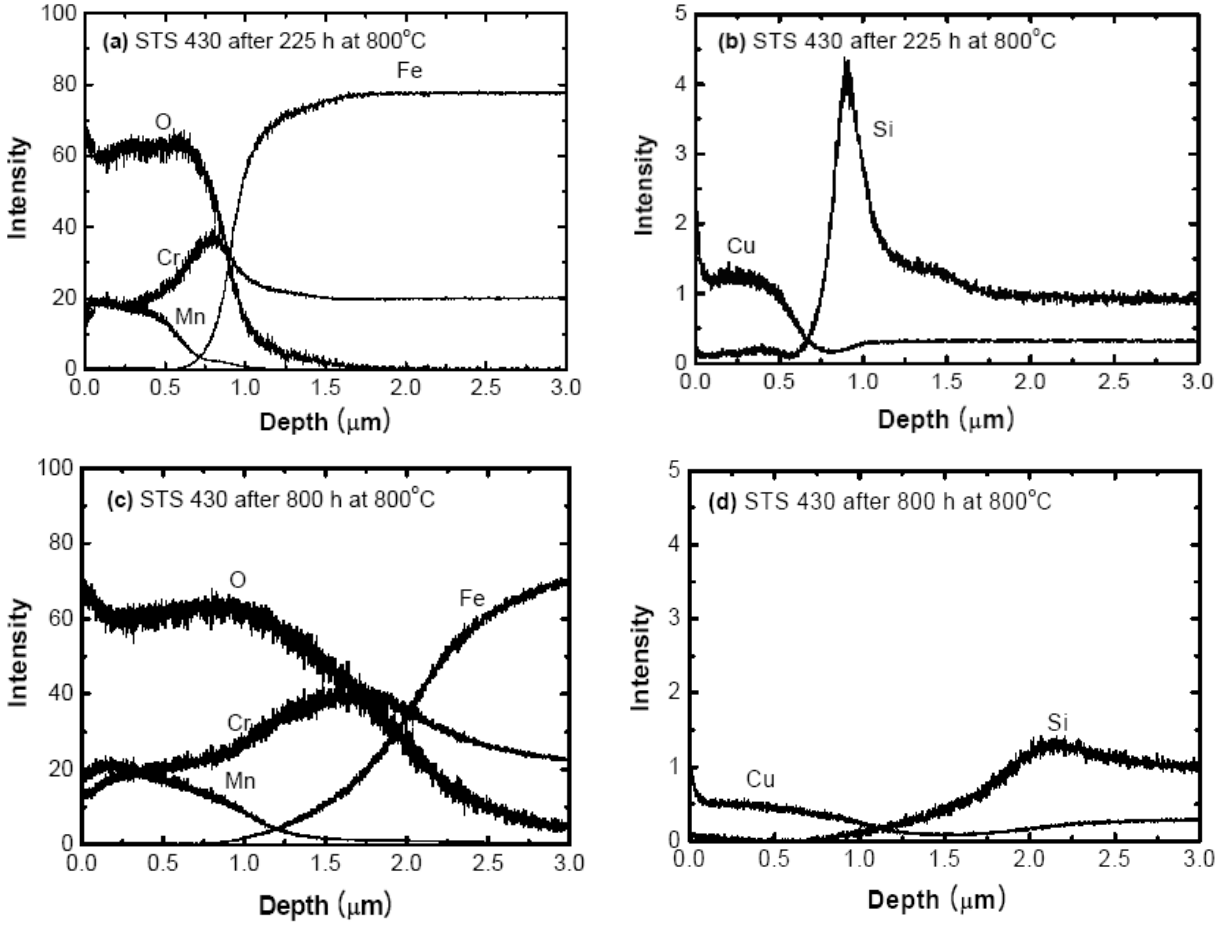

Fig. 5. GDS depth profiles for elemental distributions in the scales grown on STS 430 after oxidation at 800℃ for (a, b) 225 and (c, d) 800 h. The distributions of the major elements are shown in (a) and (c) whereas those of the minor elements are shown in (b) and (d).

oxidation. The spinel particles grew in size with increasing oxidation time up to 400 h. After 800 h as shown in Fig. 3(b), only a few angular spinel particles could be observed and the scale evolved into a fine, agglomerated microstructure. A similar microstructural change was also observed for STS 444 but the change was more drastic. At the early stages of oxidation, as shown in Fig. 4(a), the angular spinel particles formed a discontinuous layer on top of the corundum sublayer. However, after 800 h as shown in Fig. 4(b), the angular spinel particles had completely disappeared, resulting in a fine, agglomerated microstructure. The EDX analyses indicated that the fine microstructure was mainly composed of the corundum phase.

Since the XRD analyses showed that the spinel peaks became even stronger after 800 h of oxidation, the microstructural change after 800 h of oxidation could be understood as a consequence of the corundum phase outgrown over the spinel phase, but not the decomposition of the spinel phase. In the initial stages of oxidation, Mn in the alloys is preferentially oxidized by forming the spinel phase because of its high mobility in chromia and high oxidation potential.[6),8)] As the scale grows with increasing oxidation time, the ferrite substrate adjacent to the scale will be depleted by Mn, consequently resulting in the corundum phase outgrowing over the spinel phase at extended oxidation times.

The elemental distributions during the scale formation were examined by GDS depth profiling. Fig. 5 shows the GDS depth profiles from the surface of the STS 430 samples oxidized for 225 h and 800 h, Fig. 5(a) and (c) for the major elements and Fig. 5(b) and (d) for the minor elements. The GDS depth profiles from the oxidized STS 444 samples are shown in Fig. 6 for comparison with those in Fig. 5. At least three points can be realized from the elemental distributions shown in Fig. 5 and 6. First, as seen from the Cr distribution of which the peak maximum occurred beneath the surface region with high Mn contents,

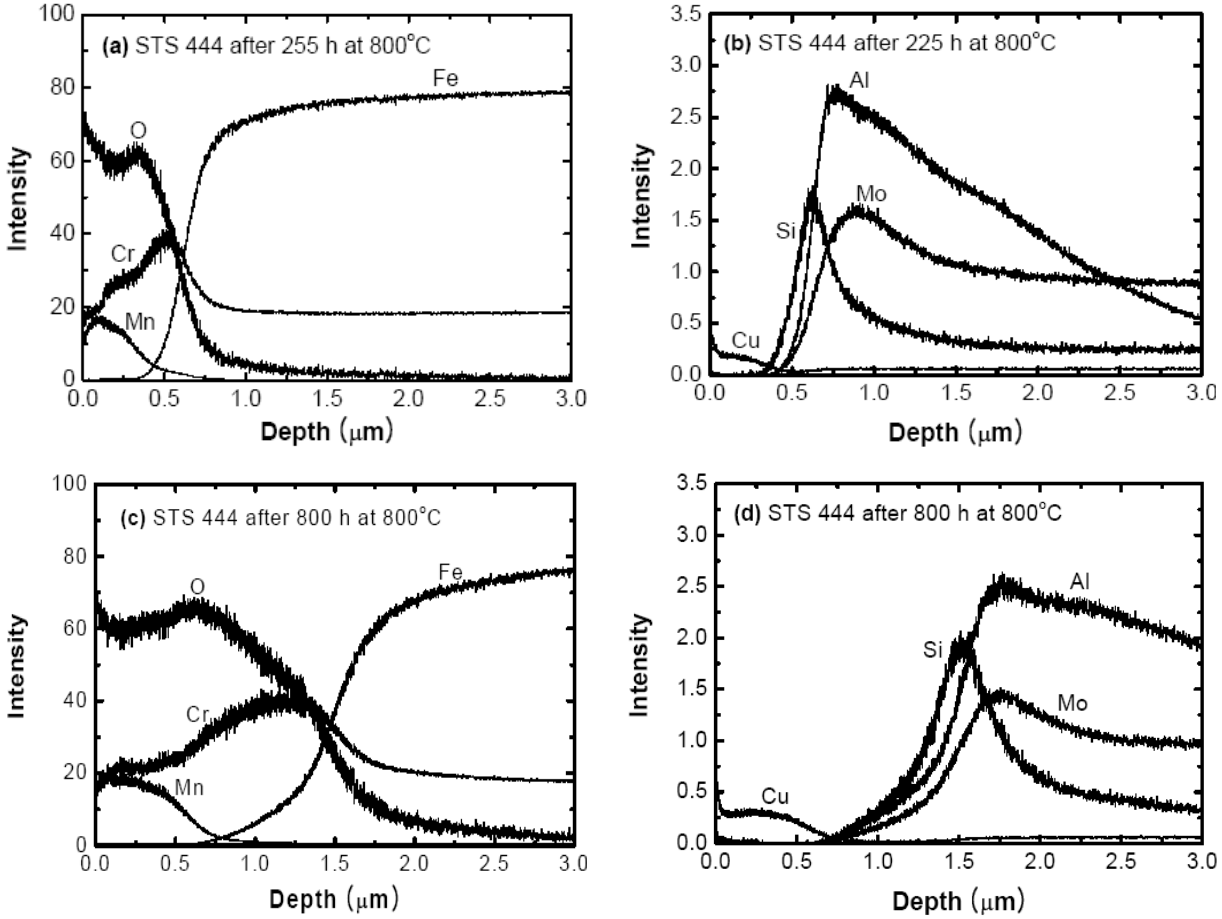

Fig. 6. GDS depth profiles for elemental distributions in the scales grown on STS 440 after oxidation at 800℃ for (a, b) 225 and (c, d) 800 h. The distributions of the major elements are shown in (a) and (c) whereas those of the minor elements are shown in (b) and (d).

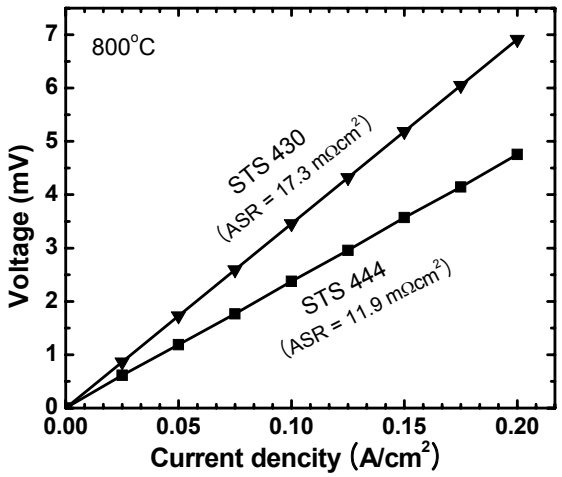

Fig. 7. Plots of voltage versus current density, as measured at 800℃, for STS 430 and STS 444 after oxidation at 800℃ for 800 h.

the oxide scales could be divided into two layers: a top layer comprised mainly of the spinel phase and a sublayer of the corundum phase. This is in accordance with previous observations.[5)-8)] Cu was preferentially incorporated into the top layer, although it was not detected by EDX due to the resolution limit. Second, in accordance with the results from the weight gain measurements, the scale growth rate was greater on STS 430 than on STS 444, resulting in the scale thicknesses of ~2.0 μm on STS 430 and ~1.5 μm on STS 444 after 800 h of oxidation. Finally, accumulation of minor elements, mainly Si for STS 430 and Si, Al, and Mo for STS 444, occurred at the scale/base metal interface. It is thought that the accumulated Si and Al atoms are likely in oxide molecules formed by internal oxidation. Because silicon and aluminum oxides exhibit poor electrical conductivities even at elevated temperatures, the formation of such oxides are expected to lower the area specific resistance. It is, however, noted that the strong adherence of the scale to the base metal for STS 444 can be attributed to the accumulation of Al and Mo.

Fig. 8 shows the results of the ASR measurements of the STS 430 and STS 444 samples oxidized for 800 h. From the linear plots of voltage and current density that demonstrated the ohmic behavior of the oxide scales, the ASR values for the scales grown on STS 430 and STS 444 were determined to be 17.3 mΩ · cm^2 and 11.9 mΩ · cm^2, respectively. $(Mn,Cr)_3O_4$ spinel is known to be more electrically conductive than Cr_2O_3.[6)] Furthermore, the electrical conductivity of the $(Mn,Cr)_3O_4$ spinel phase is known to increase with increasing the Mn contents in the phase.[9)] Nevertheless, the lower ASR value for the STS 444 sample is likely due to a smaller scale thickness and a stronger scale/metal interface.

4. Conclusions

Two kinds of commercial ferritic stainless steels, STS 430 and STS 444, were examined for the oxidation behavior and electrical properties as exposed in a wet air (3% H_2O) at 800 ℃ for times up to 800 h. The results are summarized as follows:

(1) STS 444 exhibited a lower scale growth rate with the parabolic growth constant of k_g=2.07×10^{-14} $g^2cm^{-4}s^{-1}$, as compared to STS 430 that had k_g=3.77×10^{-14} $g^2cm^{-4}s^{-1}$. Scale spallation was found on the STS 430 samples, but not on the STS 444 samples.

(2) The surface scales grown on both of the STS 430 and STS 444 samples consisted of a top layer, mainly comprised of $(Mn,Cr)_3O_4$ spinel particles, and a Cr_2O_3-rich sublayer. The spinel particles grown on STS 430 had higher Mn contents than those on STS 444. As the oxidation time increased from 400 h to 800 h, the scale surfaces of both alloys evolved into fine, agglomerated microstructures, suggesting the outgrowth of the corundum phase over the spinel phase at extended oxidation times.

(3) Strong accumulation of Si was observed at the scale/metal interfaces of both alloys. For the case of STS 444, Al and Mo, in addition to Si, were also accumulated in the base metal adjacent the scale. This accumulation of Al and Mo might be responsible for the stronger scale adherence to the base metal for the case of STS 444.

(4) After oxidation for 800 h, the ASR values of STS 430 and STS 444 were 17.3 mΩ · cm^2 and 11.9 mΩ · cm^2, respectively. The lower ASR for STS 444 was attributed to a smaller scale thickness and a stronger scale/metal interface compared to the case of STS 430.

References

1. T. Brylewski, M. Nanko, T. Maruyama, and K. Przybylski, *Solid State Ionics*, **143**, 131 (2001).
2. W. Z. Zhu and S. C. Deevi, *Mater. Sci. Eng.*, **38**, 957 (2003).
3. H. Tu and U. Stimming, *J. Power Sources*, **127**, 284 (2004).
4. K. Huang, P. Y. Hou, and J. B. Goodenough, *Solid State Ionics*, **129**, 237 (2000).
5. Z. Yang, K. S. Weil, D. M. Paxton, and J. W. Stevenson, *J. Electrochem. Soc.*, **150**, A1188 (2003).
6. Z. Yang, J. S. Hardy, M. S. Walker, G. Xia, S. P. Simner, and J. W. Stevenson, *J. Electrochem. Soc.*, **151**, A1825 (2004).
7. T. Horita, Y. Xiong, K. Yamaji, N. Sakai, and H. Yokokawa, *J. Electrochem. Soc.*, **150**, A243 (2003).
8. W. Qu, L. Jian, D. G. Ivey, and J. M. Hill, *J. Power Sources*, **157**, 335 (2006).
9. X. Chen, P. Y. Hou, C. P. Jacobson, S. J. Visco, and L. C. De Jonghe, *Solid State Ionics*, **176**, 425 (2005).